2.9 Nonuniform potential vorticity.

Our discussion of semigeostrophic models has largely been restricted to flows with uniform potential vorticity q^*. The only waves supported by such flows are the two Kelvin waves, or their frontal relatives. As noted in Section 2.1, the introduction of a potential vorticity gradient gives rise to a new restoring mechanism and a new class of waves that are nondispersive at long wave lengths. We discussed the case of topographic Rossby waves in a channel with a constant bottom slope $\partial h^*/\partial x^* = -S$ and a rigid upper boundary. The dispersion relation (2.1.30) governing a long wave propagating on a background state of rest can be generalized to include a uniform background velocity V, in which case the wave speed becomes

$$c^* = V + \left(\frac{dq^*}{dx^*}\right)\frac{w^{*2} D}{n^2\pi^2}, \quad n = 1,2,3,\cdots \tag{2.9.1}$$

where $\frac{dq^*}{dx^*} = -\frac{Sf}{D^2}$. For positive S, $\partial q^*/\partial x^* < 0$ and higher potential vorticity is found on the left-hand side (facing positive y^*) of the channel. In this case the propagation tendency of the waves is against the background flow. The latter is hydraulically critical (c^*=0) when

$$V = \frac{Sfw^{*2}}{Dn^2\pi^2}. \tag{2.9.2}$$

In the opposite case ($\partial q^*/\partial x^* > 0$), all waves propagate towards positive y^*. Critical flow for this example therefore requires that the potential vorticity increase to the left of the flow direction.

Readers versed in the dynamics of large scale flows in the ocean and atmosphere might choose to express (2.9.2) in the form

$$\frac{V}{\beta L^2} = 1,$$

where $\beta = Ddq^*/dx^*$ is a measure of the potential vorticity gradient and $L=w^*/n\pi$ is the horizontal length scale. The dimensionless parameter $V/\beta L^2$, sometimes called the *beta Froude number*, is generally interpreted as a measure of nonlinearlity of the flow field, values <<1 indicating linear dynamics. In the present context, the parameter is an indication of the importance of advection and its value must be O(1) for hydraulic effects to be possible. Various forms of the beta Froude number will arise throughout the remainder of the book in discussions of flows dominated by potential vorticity dynamics.

The presence of a potential vorticity gradient in combination with a free surface or interface leads to analytical difficulties in connection with the cross-stream structure equation (2.1.14). The difficulty can be described by first noting the connection between ψ and d implied by the geostrophic relation:

$$\frac{\partial \psi}{\partial x} = vd = \tfrac{1}{2}\frac{\partial d^2}{\partial x} + d\frac{\partial h}{\partial x}$$

If $\partial h/\partial x = 0$, integration of this equation from the channel side wall at $x=w/2$ to a point in the interior yields

$$\psi = Q + \tfrac{1}{2}(d^2 - d^2(\tfrac{1}{2}w, y)) \qquad (2.9.3)$$

where $\psi=Q$ has been imposed at $y=w/2$. Equation (2.1.14) may now be written as

$$\frac{\partial^2 d}{\partial x^2} - q[Q - \tfrac{1}{2}(d^2 - d^2(\tfrac{1}{2}w, y))]d = -1 \qquad (2.9.4).$$

If q is constant (2.9.4) reduces to the familiar linear equations that form the basis for models considered earlier. However, a nontrivial dependence of q on ψ introduces a nonlinearity that generally precludes analytical solutions for the cross-channel structure.

a. Stern's criterion.

Some progress can be made without actually solving the particulars of the cross-stream structure. For example, Stern (1974) derives a generalized critical condition with no restriction on potential vorticity and with the requirements that the channel cross-section be rectangular $(\partial h/\partial x = 0)$ and that the flow be unidirectional. A version of the proof, grounded in Stern's approach but simpler than his original proof, begins with the relation

$$v = \pm 2^{1/2}[B(Q + \tfrac{1}{2}(d^2 - d^2(\tfrac{1}{2}w, y))) - d - h]^{1/2}$$

which follows from the definition of the semigeostrophic Bernoulli function $B(\psi)$ and from (2.9.3). Assume that the velocity is positive, so that the '+' sign is appropriate. If this v is substituted into the geostrophic relation, essentially $\partial d / v = \partial x$, and the result integrated across the channel width, one obtains

$$
\begin{aligned}
w &= \int_{-w/2}^{w/2} dx = \int_0^Q \frac{dx}{d\psi} d\psi = \int_0^Q \frac{1}{vd} d\psi \\
&= \int_0^Q \frac{1}{2^{1/2} d[B(\psi) - d - h]} d\psi \qquad (2.9.5) \\
&= \int_{\left[d^2(\frac{1}{2}w,y) - 2Q\right]^{1/2}}^{d(\frac{1}{2}w,y)} \frac{\partial d}{2^{1/2}[B(Q + \frac{1}{2}(d^2 - d_{-w/2}^2)) - d - h]}
\end{aligned}
$$

The use of d as an integration variable assumes a one-to-one correspondence between x and d, and this is guaranteed when v remains positive for $-w/2 \le x \le w/2$. The lower limit of integration is the left wall depth expressed in terms of the flow rate and the right wall depth. If $B(\psi)$ is known in advance, then the first and last of (2.9.5) can be combined to form the hydraulic functional

$$
\mathcal{G}(d_{-w/2}; w; Q) = \int_{\left[d^2(\frac{1}{2}w,y) - 2Q\right]^{1/2}}^{d(\frac{1}{2}w,y)} \frac{\partial d}{2^{1/2}[B(Q + \frac{1}{2}(d^2 - d_{-w/2}^2)) - d - h]} - w = 0
$$

expressing a relationship between the single dependent variable $d(\frac{1}{2}w, y)$, the geometric variables w and h, and the parameter Q. A critical condition can thus be obtained by taking $\partial \mathcal{G} / \partial d(\frac{1}{2}w, y) = 0$. After use of Leibnitz's Rule and some careful integration by parts, one obtains the result

$$
\int_{\left[d^2(\frac{1}{2}w,y) - 2Q\right]^{1/2}}^{d(\frac{1}{2}w,y)} \left(\frac{1}{dv_+^{\,3}} - \frac{1}{d^2 v_+} \right) \partial d = 0 .
$$

Changing the integration variable from d to x (using $\partial d = v \partial x$) leads to Stern's result, which can be written in dimensional terms as

$$
\int_{-w^*/2}^{w^*/2} \frac{1}{v^{*2} d^*} \left(1 - \frac{v^{*2}}{g d^*} \right) dx^* = 0 . \qquad (2.9.6)
$$

In essence, the local value of the Froude number $v^* / \sqrt{g d^*}$ must be 1 for some x^* across the channel in order for the flow to be critical. It is remarkable that this result does not depend on the Coriolis parameter f. It is also interesting that (2.9.6) appears to apply to potential vorticity waves as well as Kelvin and frontal waves. However, the restriction to unidirectional velocity profiles may disallow certain types of critical states, an issue that we will return to. As an aside, we note that the same reasoning that results in (2.9.6) can be used to estimate the speeds of certain long waves a given flow. This subject is taken up in Exercise 3.

Stern's result can be used to define a type of generalized Froude number

$$F_d = \frac{\int_{-w^*/2}^{w^*/2} \frac{1}{gd^{*2}} dx^*}{\int_{-w^*/2}^{w^*/2} \frac{1}{d^* v^{*2}} dx^*} \tag{2.9.7}$$

having the property that F_d=1 for critical flow and $F_d \to 0$ as $v^* \to 0$. The latter limit implies that F_d<1 for subcritical flow, but one should exercise caution in making this interpretation. Flows with nonuniform potential vorticity may admit to many wave modes and a particular value of F_d does not, in itself, indicate supercritical or subcritical conditions with respect to all possible waves. We only know that F_d=1 indicates that one of the waves is arrested.

$$\int_{-w^*/2}^{w^*/2} \frac{1}{(v^* - c^*)^2 d^*} \left(1 - \frac{(v^* - c)^2}{gd^*} \right) \partial x^* = 0$$

b. The solution of Pratt and Armi.

A detailed example of hydraulic effects in the presence of both gravitational and potential vorticity dynamics was worked out by Pratt and Armi (1987). In order to make the problem analytically tractable, they examined a nonrotating flow with the linear potential vorticity distribution

$$q^*(\psi^*) = q_o^* - a\psi^*, \tag{2.9.8}$$

in a channel with rectangular cross section. Although f=0 this flow supports both gravity and potential vorticity waves and therefore contains some of the essential features we wish to investigate. Simplicity is provided by the fact that the d^* is uniform across the channel, $d^*=d^*(y^*)$, so that the expression for potential vorticity reduces to

$$q^* = \frac{\partial v^* / \partial x^*}{d^*} \tag{2.9.9}.$$

Differentiation with respect to x^* and use of (2.9.8) leads to the cross-stream structure equation

$$\frac{\partial^2 v^*}{\partial x^{*2}} + ad^{*2} v^* = 0\,. \tag{2.9.10}$$

There are two distinct cases to consider. When $a<0$, $dq^*/d\psi^* < 0$ and the potential vorticity has higher values on the right side of the channel (where $\psi^*=Q^*/2$) then on the left side (where $\psi^*=-Q/2$), although the variation of q^* across the channel may not be monotonic. As suggested in Figure 2.9.1a, this setting would seem to favor potential vorticity wave propagation in the same direction as the overall transport. In this case the solutions to (2.9.10) will be exponential. If $a>0$ the situation is as shown in Figure 2.9.1b, with generally higher potential vorticity on the left and possible upstream propagation of potential vorticity waves. Here the solutions to (2.9.10) are oscillatory.

Consider the case $a<0$ first. The solution to (2.9.10) can be written as

$$v^* = \frac{\hat{v}^* \sinh(\alpha x^*)}{\sinh(\frac{1}{2}\alpha w^*)} + \frac{\bar{v}^* \cosh(\alpha x^*)}{\cosh(\frac{1}{2}\alpha w^*)}, \qquad (2.9.11)$$

where

$$\alpha(y^*) = |a|^{1/2} d^*(y^*),$$

$$\bar{v}^*(y^*) = \tfrac{1}{2}[v(\tfrac{1}{2}w^*, y^*) + v(-\tfrac{1}{2}w^*, y^*)],$$

and

$$\hat{v}^*(y^*) = \tfrac{1}{2}[v(\tfrac{1}{2}w^*, y^*) - v(-\tfrac{1}{2}w^*, y^*)].$$

As in Gill's (1977) model the flow has a boundary layer structure, each layer here having thickness α^{-1}. However there are some important differences. One is that the decay scale depends only on the magnitude of the potential vorticity gradient $|\alpha| = |dq^*/d\psi^*|$ and the depth d^*, and not on gravity.[1] Furthermore, the decay scale *depends on the dependent variable d* and is therefore a function of y, whereas Gill's decay scale (L_d) was universally constant.

The boundary conditions $\psi^*(\pm\frac{1}{2}w^*) = \pm\frac{1}{2}Q^*$ may be used to relate $\hat{v}^*$, $\bar{v}^*$ and d^* and form a hydraulic functional. The first step is to integrate the product of d^* and (2.9.11) across the channel, resulting in

$$\bar{v}^* = \frac{\alpha Q^* \coth(\frac{1}{2}\alpha w^*)}{2d^*}. \qquad (2.9.12)$$

Next, the potential vorticity equation (2.9.9) is applied at $x^*=w^*/2$, leading to $\partial v^*/\partial x = d^*(q_o^* - \frac{1}{2}aQ^*)$. The use of (2.9.11) to evaluate $\partial v^*/\partial x^*$ there results in

---

[1] • The decay scale can also be written as $\left|\frac{v^*}{dq^*/dy^*}\right|^{1/2}$ which may be compared with the thickness $\left(\frac{V}{\beta}\right)^{1/2}$ of inertial boundary currents on a beta-plane ocean (Charney, 1955). Here V is velocity scale and β is the planetary potential vorticity gradient.

$$\hat{v}^* = d^* q_o^* \alpha^{-1} \tanh(\tfrac{1}{2}\alpha w^*). \qquad (2.9.13)$$

Finally a functional relation of the required form is obtained by evaluating the Bernoulli equation along the right-hand wall:

$$\tfrac{1}{2}(\bar{v}^* + \hat{v}^*)^2 + d^* + h^* = B_R^*. \qquad (2.9.14)$$

Here B_R represents the right-wall value of the Bernoulli function. Substitution for $\hat{v}^*$ and $\bar{v}^*$ and nondimensionalization of the result leads to

$$\mathcal{G}(d;h,w) = \tfrac{1}{2}\left[\frac{1}{\tanh(\gamma d)} + \frac{\tanh(\gamma d)}{\Delta q}\right]^2 + d + h - B_R = 0 \qquad (2.9.15)$$

where $(d,h,B_R) = (d^*/D, h^*/D, B_R^*/gD)$ and

$$\gamma = \tfrac{1}{2} w^* |a|^{1/2} D, \qquad (2.9.16)$$

$$D = \frac{|a| Q^{*2}}{4g}, \qquad (2.9.17)$$

and

$$\Delta q = \frac{|a| Q^*}{2 q_o^*}, \qquad (2.9.18)$$

all of which are non-negative.

$\mathcal{G}(d;h,w)$ contains two parameters γ and Δq. The former is one half the ratio of the channel width to the boundary layer width based on the scale depth *D*.
It is a measure of the strength of potential vorticity effects over the cross-section of the flow. If $\gamma << 1$ potential vorticity effects are relatively weak. The other parameter Δq is a measure of the relative importance in the two terms q_o^* and $a\psi^*$ which comprise the potential vorticity. Specifically, Δq is the difference between the potential vorticity at the right and left walls normalized by their sum.

The critical condition $\partial \mathcal{G} / \partial d = 0$ leads to

$$\gamma \sinh(\gamma d_c)\operatorname{sech}^3(\gamma d_c)[\coth^4(\gamma d_c) - \Delta q^{-2}] = 1 \qquad (2.9.19)$$

and the left-hand side of this expression decreases monotonically from positive ∞ to zero, indicating at most a single root. A typical solution curve (Figure 2.9.2), based on (2.19.15) with the width *w* held constant, shows a single minimum in the value of B_R-*h* plotted as a function of *d* with . Solutions are constructed in the usual way by following the curve as *h* changes. A hydraulic transition occurs if the maximum *h*

coincides with the minimum of the curve. It can be shown that, in the limit of vanishing Δq and γ, (2.9.19) reduces to the result for one-dimensional flow: $\bar{v}^* = v^* = (gd^*)^{1/2}$. In this limit the left- and right-hand branches of the solution curves correspond respectively to supercritical and subcritical flows. We will assume that this characterization continues to hold for non-zero Δq and γ with the caveat that the actual wave speeds along the two branches have not been calculated.

There is nothing so far that dramatically distinguishes the character of the model from its one-dimensional counterpart. However, a closer look at the velocity structure reveals an important difference, namely that stagnation points with corresponding separating streamlines can exist on the left-hand wall. The required condition is $\hat{v}^* = \bar{v}^*$, or if (2.9.12) and (2.9.13) are used:

$$\Delta q = \tanh^2(\gamma d_s). \tag{2.9.20}$$

Here d_s denotes the value of d at the section of wall stagnation. The corresponding right-wall condition is obtained by reversing the sign of the right-hand term and cannot be satisfied for positive Δq. Hence, stagnation can occur only on the left wall. The use of (2.9.20) to substitute for Δq in the critical condition, (2.9.19) leads to

$$\gamma \frac{\sinh(\gamma d_c)}{\cosh^3(\gamma d_c)}[\coth^4(\gamma d_c) - \coth^4(\gamma d_s)] = 1, \tag{2.9.21}$$

and thus d_c must be $<d_s$ (the flow must be subcritical) for separation to occur. This *stagnation* separation should be distinguished from the rotation induced separation in which the wall depth vanishes. In Figure 2.9.2, subcritical solutions with $d>d_s$ are indicated by dashing. In this case, most of the subcritical curve has this property. Corresponding velocity profiles (Figure 2.9.3) will have reverse flow along the left-hand wall. The three sections correspond to points A, B, and C of the solution curve. Immediately upstream of the sill lies the stagnation point and beyond it a counterflow. At section A most of the channel contains recirculating fluid; only that passing close to the right wall reaches the sill.

We now turn to the more interesting case *a>0,* which is favorable for potential vorticity wave propagation against the mean flow. The solution to (2.9.10) is

$$v^* = \hat{v}^* \frac{\sin(\alpha x^*)}{\sin(\alpha w^*/2)} + \bar{v}^* \frac{\cos(\alpha x^*)}{\cos(\alpha w^*/2)}, \tag{2.9.22}$$

so that the velocity profile is oscillatory. Repetition of the earlier procedure leads to

$$\bar{v}^* = \frac{\alpha Q^* \cot(\alpha w^*/2)}{2d^*} \tag{2.9.23}$$

and

$$\hat{v}^* = \frac{q_o^* d^* \tan(\alpha w^*/2)}{\alpha}. \qquad (2.9.24)$$

Substitution of (2.9.23) and (2.9.24) into the Bernoulli equation (2.9.14) and nondimensionalization gives

$$\mathcal{G}(d;h,w) = \tfrac{1}{2}[\cot(\gamma d) + \frac{\tan(\gamma d)}{\Delta q}]^2 + d + h - B_R = 0 \qquad (2.9.25)$$

where γ and Δq are defined as before and are considered positive. Note that the squared term has the value $+\infty$ for $\gamma d = \frac{1}{2} n\pi$ $(n = 0,1,2,\cdots)$, suggesting that the solution 'curve' consists of a series of disconnected lobes. This is confirmed by a plot (Figure 2.9.4) showing $B_R - h$ as a function of d for $\gamma = \Delta q = 1$. Note that the minimum value of $B_R - h$ increases as the lobe number increases. For a given upstream state (here determined by B_R) and a given topographic elevation h, there may be more than two possible steady states. For example the value $B_R - h = 10$ corresponds to 12 possible states. However, once a particular solution lobe is determined, perhaps on the basis of further information about the upstream state, then at most two states are possible for any given h. Of course, a hydraulic jump or some other non-conservative feature might allow the solution to switch from one lobe to another, thereby allowing more possibilities.

Stagnation along the left wall is also possible and occurs when $\hat{v}^* = \bar{v}^*$, or

$$\Delta q = \tan^2(\gamma d_s). \qquad (2.9.26)$$

As before, separation along the right wall is not possible for non-zero Δq.

At the minimum of each lobe the flow is critical and the corresponding depth d_c can be calculated from the condition $\partial \mathcal{G} / \partial d = 0$, which yields

$$\gamma \frac{\sin(\gamma d_c)}{\cos^3(\gamma d_c)}[\cot^4(\gamma d_c) - \cot^4(\gamma d_s)] = 1. \qquad (2.9.27)$$

It can be shown using (2.9.6) and (2.9.7) that $d_s > d_c$ within each lobe.

The most obvious qualitative difference between solutions corresponding to different lobes is in the number of zero crossings of the cross-channel profile of v. It can be shown that the solutions corresponding to lobe n have either n or n-1 zero crossings, the greater number occurring for larger values of d. Thus the higher lobes correspond to intricate flows with multiple bands of fluid moving upstream and downstream. Figures 2.9.5 and 2.9.6 show examples taken from lobes #1 and #2.

There remains some mystery concerning solutions corresponding to different solution lobes. If the cross-channel solution is reduced by taking the limits γ and $\Delta q \rightarrow 0$, lobe #1 tends toward the solution curve for a one-dimensional, nonrotating flow (e.g. Figure 1.4.1). The inset of Figure 2.9.4 shows how this limit is approached: as γ and Δq are reduced, the depth range of the first lobe grows and the remaining lobes are pushed off to infinity. Controlled solutions belonging to the first lobe appear then to be governed by the dynamics of a shear-modified, long gravity wave. For the other solutions, it is evident that the relative change in depth across the sill are relatively small and becomes vanishingly so for the higher lobes. The change in the flow as it passes through a critical section is primarily one of horizontal structure. This idea can be formalized by clculation of the cross sectional enstrophy

$$E_n^* = \tfrac{1}{2} \int_{-w^*/2}^{w^*/w} \left(\partial v^*/\partial x^*\right)^2 dx = \tfrac{1}{2} d^{*2} \int_{-w^*/2}^{w^*/w} q^{*2}\, dx\,, \qquad (2.9.28)$$

a measure of the horizontal shear across a particular section. As explored in Exercise 3 it can be shown that the change in E_n^* caused by a small change in depth as the flow passes through a critical section increases as the lobe number becomes higher. This indicates that control of the flow corresponding to higher lobes primarily affects the horizontal shear and not the depth. Because of this feature, and because the higher lobes owe their presence entirely to a finite potential vorticity gradient, it is evident that the corresponding solutions are controlled by a potential vorticity wave.

Further to the ongoing discussion, it can be shown that Stern's condition for criticality (2.9.6) succeeds in predicting the control condition for the first lobe, but fails for the remaining lobes. Failure is due to the fact that the higher lobe solutions all have velocity reversals, whereas the derivation of (2.9.6) assumes unidirectional flow. Flows with potential vorticity gradients may therefore experience a multiplicity of controlled configurations, not all of which obey Stern's criterion.

A final consideration, one that could render much of the above discussion academic, is stability. The most pertinent theorem for the present case is Fjortoft's necessary condition for instability (see Drazin and Reid, 1981), which does not strictly apply to our flow in general, but would be applicable if the flow were bounded by a rigid lid. Instability is possible when $dq^*/d\psi^* < 0$, or $a > 0$, the case permitting multiple solutions.

There remains uncertainty regarding the interpretation of the $a > 0$ solutions, how they are established, which branches of the higher lobes are supercritical and subcritical, and what their stability is. One of the difficulties is that the model contains a mix of potential vorticity and gravity wave dynamics. More recent investigations of hydraulic effects in the presence of potential vorticity gradients have utilized models that expunge gravity waves by placing a rigid lid on the surface. Also, piecewise constant (rather than continuous) distributions of q^* can reduce the number of wave modes to just one or two, further simplifying the problem and allowing the peculiar dynamics to be investigated in

isolation. These models take us away from the topics and applications of the current chapter, but they are revisited in Chapter 6.

c. Killworth's solution.

Abyssal flows that occur in deep ocean basins tend to be slow and nearly geostrophic, and perhaps not of the character envisioned by WLK and Gill in the upstream basins of their models. In an attempt to pose more realistic upstream conditions, Kllworth (1992) considered an inviscid model with a broad, geostrophically balanced basin flow over a horizontal bottom. As it turns out, this assumption is sufficient to determine the potential vorticity of the flow, which turns out to be nonuniform.

The starting point is the assumption that the upstream velocity is nondimensionally small (v<<1). The expressions for the potential vorticity and Bernoulli functions then reduce as follow:

$$q(\psi) = \frac{1 + \partial v / \partial x}{d} \cong \frac{1}{d}$$

and

$$B(\psi) = \frac{v^2}{2} + d + h \cong d\,,$$

assuming that h=0 in the upstream reservoir. When combined with (2.9.3), these two relations yield

$$B(\psi) = \left[2(\psi - Q) + d^2(\tfrac{1}{2}w, -\infty) \right]^{1/2} \qquad (2.9.29)$$

and

$$q(\psi) \cong \left[2(\psi - Q) + d^2(\tfrac{1}{2}w, -\infty) \right]^{-1/2},$$

where $d(\frac{1}{2}w, -\infty)$ is the depth at the right wall of the reservoir.

If the flow drains into a narrow and/or shallow channel and develops O(1) velocities, it is constrained by the semigeostrophic equations. In particular, the flow must obey the integral constraint (2.9.5), or

$$w = \int_0^Q \frac{1}{2^{1/2} d[B(\psi) - d - h]} d\psi \qquad (2.9.30)$$

With $B(\psi)$ given by (2.9.29), and d given in terms of ψ by (2.9.3), (2.9.30) forms an implicit relation between w, h, and the right-wall depth $d(w/2,y)$, the single remaining

flow variable. The reader is reminded, however, that the derivation of this relation requires one-to-one relation between x and ψ, and thus flow reversals are not permitted.

Killworth (1992) solved a version of (2.9.30) and obtained standard hydraulic curves relating $d(w/2,y)$ to either h or w. All such curves are similar to those shown in Figure 2.9.4 in having a single maxima or minima, and the corresponding control is associated with Kelvin wave dynamics. The author speculates that solutions with potential vorticity wave controls may be possible, but the model would have to be extended to allow flow reversals. This is left as a project for an interested student.

d. Summary

The role of potential vorticity waves and controls in deep overflows and other gravity-driven flows remains imperfectly understood. If the potential vorticity gradient is single signed, and if high values of q lie to the left, facing downstream, then the waves attempt to propagate against the current and hydraulically critical flow is possible. The implied critical control appear to effect the horizontal vorticity of the flow field, rather than the surface or interface height. Solutions with a potential vorticity wave control appear to be disconnected from solutions that exhibit control by a gravity or Kelvin wave, or by a potential vorticity wave with a different modal structure. If the Pratt and Armi (1987) model is any indication, it does not seem to be possible to combine two types of controls within the same conservative current system. The fact that deep-ocean overflows appear to exhibit gravitational control may disqualify potential vorticity controls. The latter may, however, act in broad ocean jets or strait flows that are not controlled with respect to gravity waves. All of these comments involve conjecture, begging further investigation.

Another feature suggested by this small body of work is that the presence of a potential vorticity control requires velocity reversals across the control section. This may be connected to the modal structure of the stationary wave, which is itself wiggly. The presence of velocity reversals means that certain analytical results, including Stern's critical condition and Killworth's model, both of allow for non-uniform potential vorticity, do not allow for potential vorticity wave control. Both rely on an x-to-ψ coordinate transform, which requires a unidirectional flow.

A further cloud on the horizon is instability, which by Fjortort's theorem, is favored by the same potential vorticity distributions that allow potential vorticity wave criticality.

Exercises

1) Obtain the result (2.9.6) starting with the trivial relation

$$w = \int_{-w/2}^{w/2} dx$$

and change the integration variable x to ψ. (What does the use of this last tranformation assume about the flow?). Attempt to cast the new integral as a Gill-type functional in a single variable and use the result to obtain a critical condition.

3) Show that the velocity profile (2.9.22) can be written in the nondimensional form

$$v = \frac{\sin(\gamma dx)}{\Delta q \sin(\gamma d)} + \frac{\cos(\gamma dx)}{\cos(\gamma d)},$$

where $v = 2v^*/|a|^{1/2} q$, $d=d^*/D$, $x^*=x/(w^*/2)$ and γ is as defined above. Using this expression, calculate the nondimensional version E_n of the enstrophy E_n^* (first equality in 2.9.28). Now take the derivative of the result with respect to d and evaluate it at the critical depth. From the result, show that

$$(\partial E_n / \partial d)_{d=d_c} \sim d_c^2 \quad (d_c \to \infty),$$

and therefore the change in enstrophy relative to a change in depth increases as the critical depth (and therefore the lobe number) increases.

3. Using the results from Part *a*, show that the phase speed c^* of a long wave propagating along the (rectangular) channel is given by

$$\int_{-w^*/2}^{w^*/2} \frac{1}{(v^*-c^*)^2 d^*}\left(1 - \frac{(v^*-c)^2}{g d^*}\right) dx^* = 0,$$

provided that c^* does not lie in the range of the variation of v^*. Note for given $v^*(y^*)$ and $d^*(y^*)$, c^* will obey a quadratic equation. There are therefore only two such waves. Speculate on why the integral constraint does not capture the remaining waves.

Figure Captions

Figure 2.9.1 The direction of potential vorticity wave propagation, relative to background flow advection, for potential vorticity gradients of different signs. The channel is nonrotating and the potential vorticity gradient is determined entirely by the gradients in horizontal shear.

Figure 2.9.2 A plot of B_R-h as a function of d for a channel of constant width, and with $a<0$. The solution is based on equation (2.9.15) with $\Delta q = \gamma = 1$. The dashed section of curve corresponds to bidirectional flow. In the inset plot, γ has been reduced to 0.1.

Figure 2.9.3 Plan view of a hydraulically controlled flow. Sections A, B and C correspond to the points indicated in Figure 2.9.2.

Figure 2.9.4. A plot of B_R-h as a function of d for a channel of constant width, and with $a>0$. The solution is based on equation (2.9.25) with $\gamma=\Delta q=1$. The dashed section of curves corresponds to flows with velocity reversals. In the inset plot, γ and Δq have been reduced to 0.2.

Figure 2.9.5 Plan view of a controlled solution based on Lobe 1 of the Figure 2.9.4 solution curve. Lettered sections match points in Figure 2.9.4.

Figure 2.9.6. Same as for the previous figure, but now the solution is based on lobe 2 of the Figure 2.9.3 solution curve.

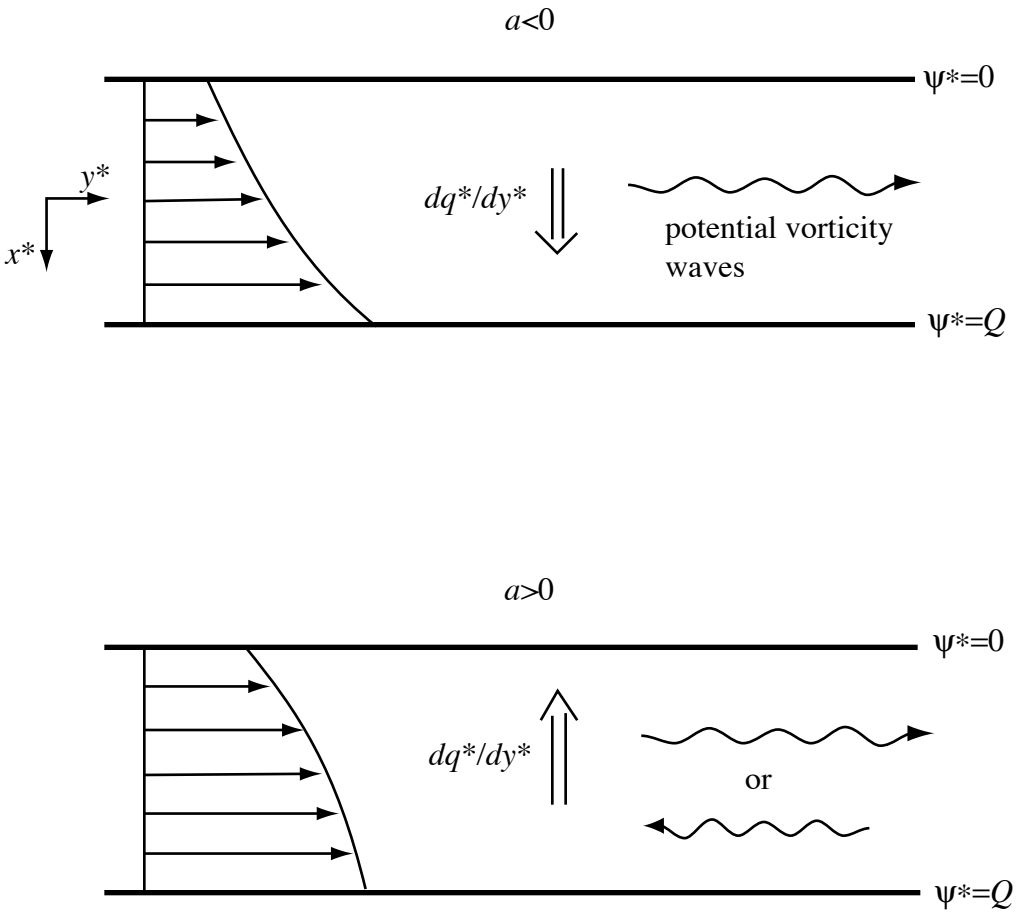

Figure 2.9.1

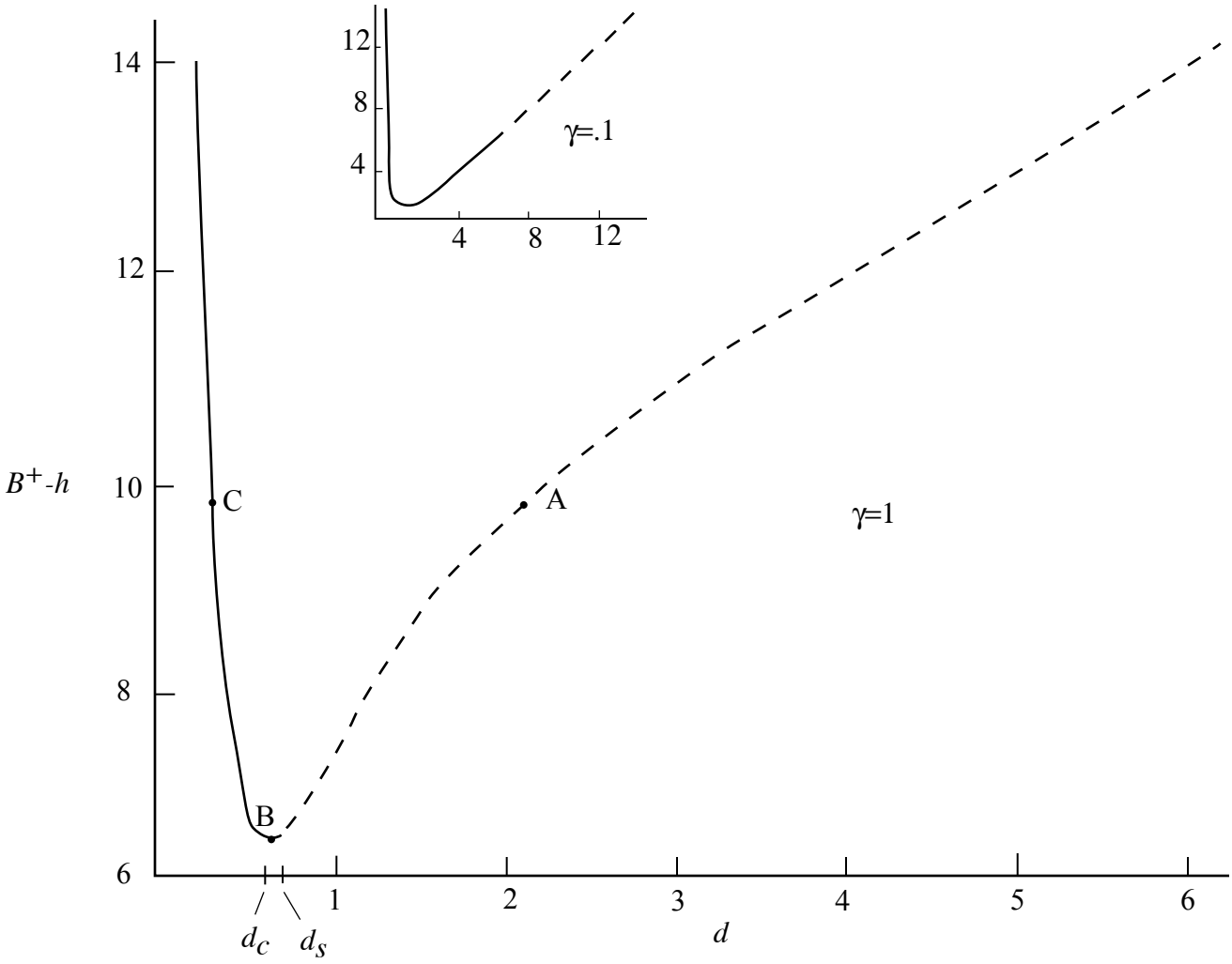

Figure 2.9.2

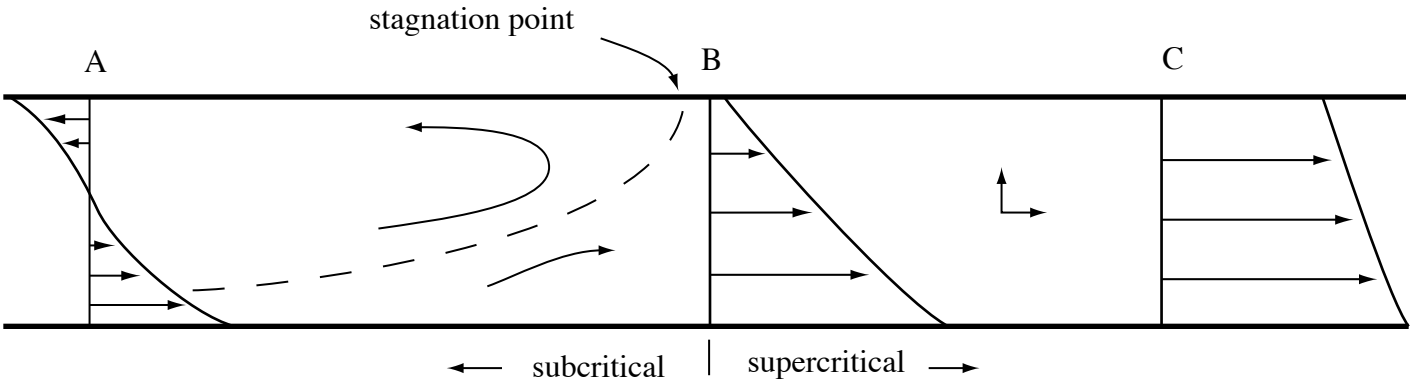
stagnation point
A
B
C
subcritical
supercritical

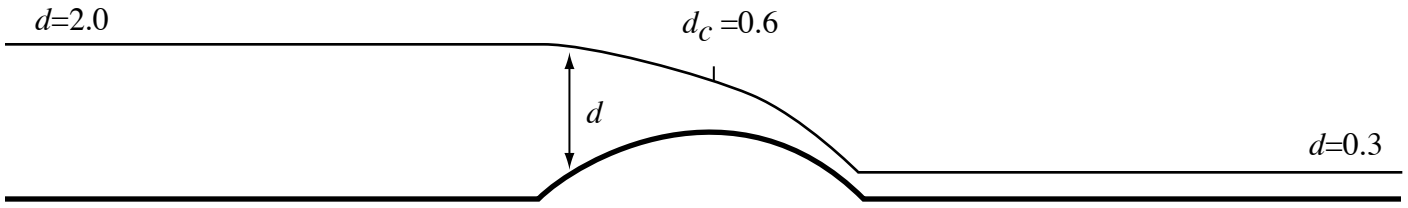
d=2.0
d_c =0.6
d
d=0.3

Figure 2.9.3

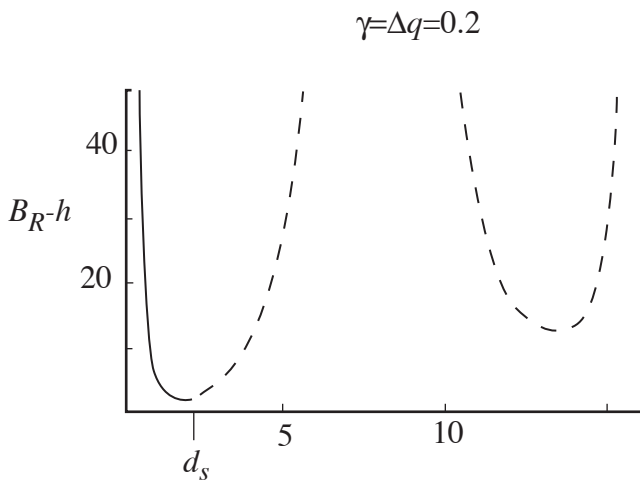
γ=Δq=0.2
40
20
B_R-h
5
10
d_s

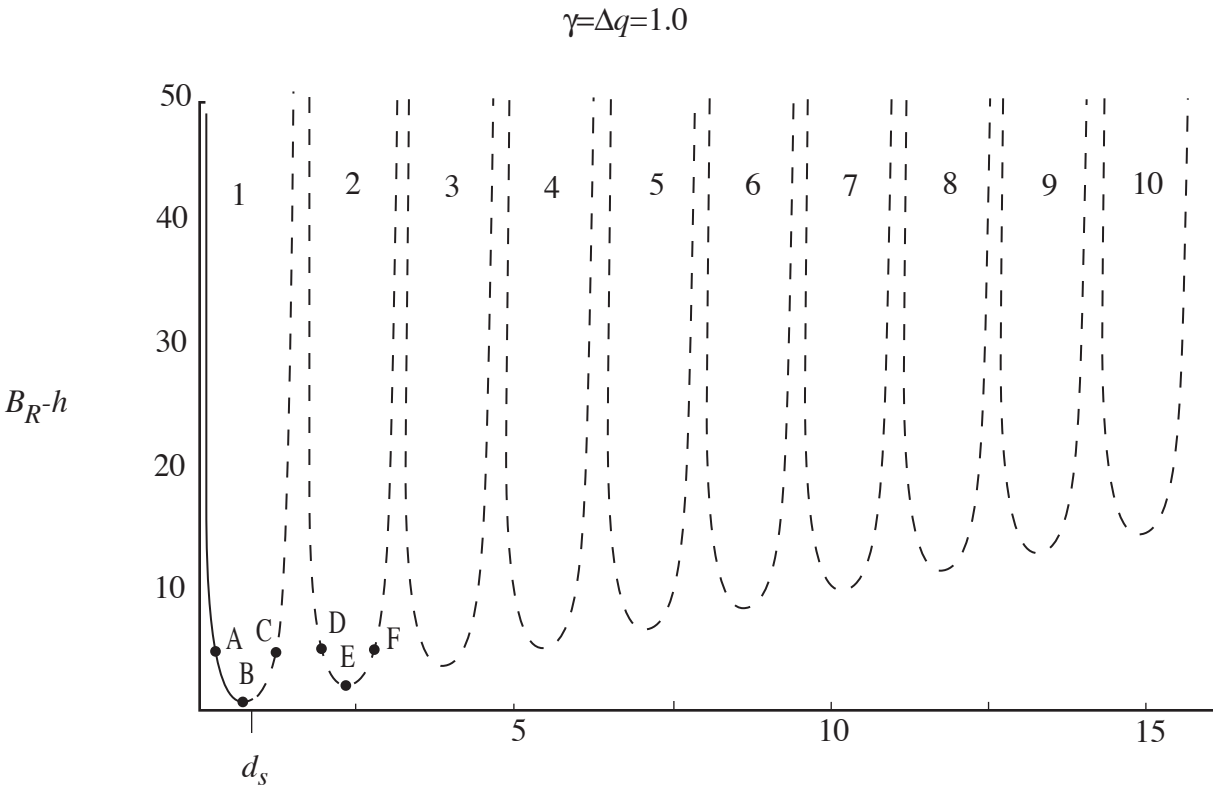
γ=Δq=1.0
50
40
30
20
10
B_R-h
1
2
3
4
5
6
7
8
9
10
A
B
C
D
E
F
5
10
15
d_s

Figure 2.9.4

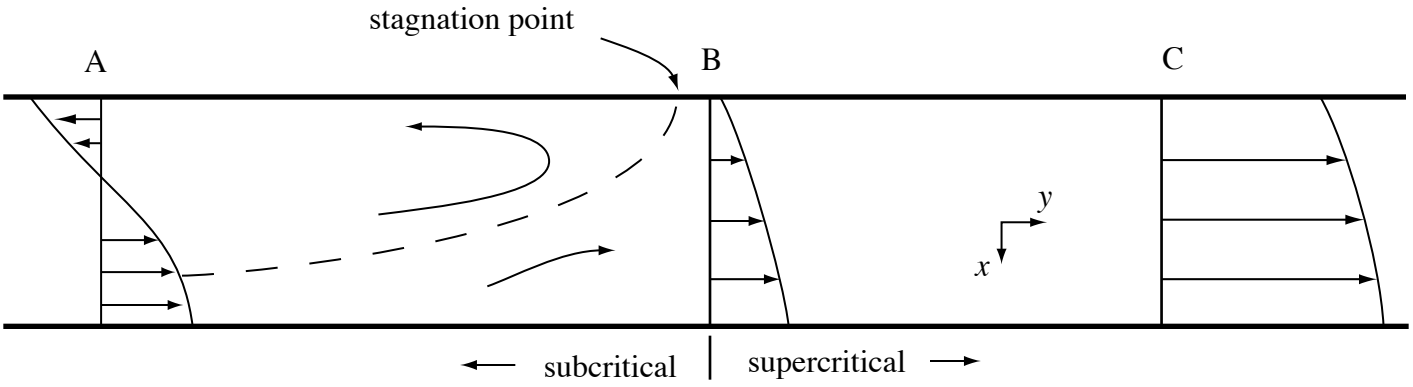
stagnation point
A
B
C
y
x
subcritical
supercritical

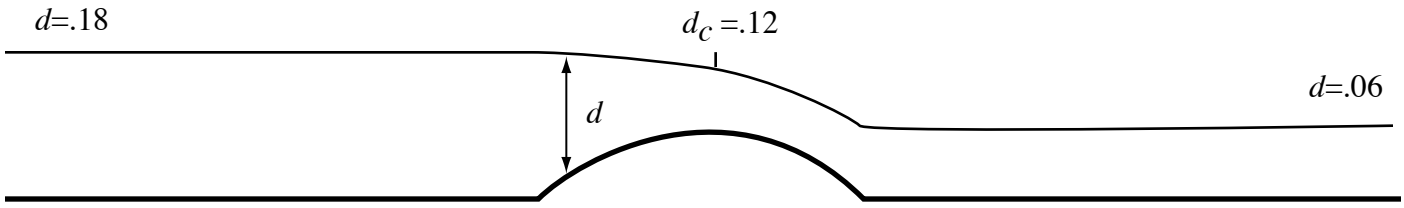
d=.18
d_c =.12
d
d=.06

Figure 2.9.5

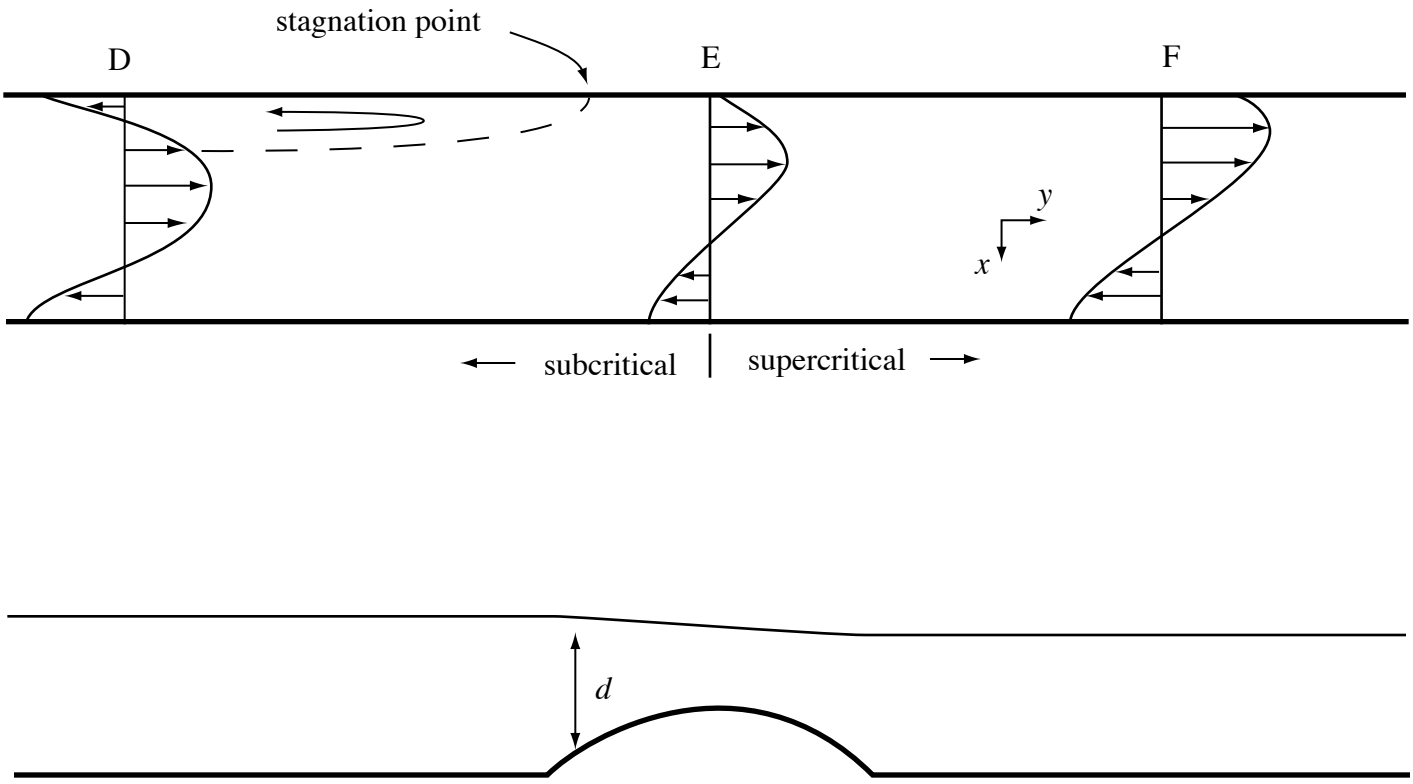

Figure 2.9.6